Journal of Materials Chemistry A c6ta08233e

PAPER

A high-performance flexible and weavable asymmetric fiber-shaped solid-state supercapacitor enhanced by surface modifications of carbon fibers with carbon nanotubes

Xiaoyu Lu, Yang Bai, Ranran Wang and Jing Sun*

A carbon fiber-based positive electrode enhanced by carbon nanotube modification with electrodeposited porous $NiCo(OH)_x$ and a negative electrode decorated with activated carbon were prepared. The assembled asymmetric fiber-shaped solid-state supercapacitor showed high energy and power densities with great weavability to be used in wearable electronics.

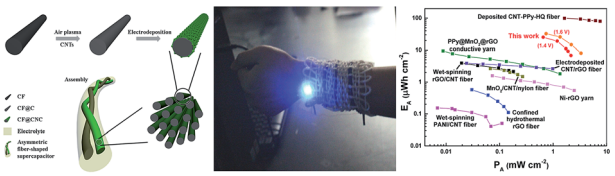

Please check this proof carefully. **Our staff will not read it in detail after you have returned it.**

Translation errors between word-processor files and typesetting systems can occur so the whole proof needs to be read. Please pay particular attention to: tabulated material; equations; numerical data; figures and graphics; and references. If you have not already indicated the corresponding author(s) please mark their name(s) with an asterisk. Please e-mail a list of corrections or the PDF with electronic notes attached - do not change the text within the PDF file or send a revised manuscript. Corrections at this stage should be minor and not involve extensive changes. All corrections must be sent at the same time.

Please bear in mind that minor layout improvements, e.g. in line breaking, table widths and graphic placement, are routinely applied to the final version.

We will publish articles on the web as soon as possible after receiving your corrections; **no late corrections will be made.**

Please return your **final** corrections, where possible within **48 hours** of receipt by e-mail to: materialsA@rsc.org

Queries for the attention of the authors

Journal: **Journal of Materials Chemistry A**

Paper: **c6ta08233e**

Title: **A high-performance flexible and weavable asymmetric fiber-shaped solid-state supercapacitor enhanced by surface modifications of carbon fibers with carbon nanotubes**

Editor's queries are marked like this... **1**, and for your convenience line numbers are inserted like this... 5

Please ensure that all queries are answered when returning your proof corrections so that publication of your article is not delayed.

Query Reference	Query	Remarks
1	For your information: You can cite this article before you receive notification of the page numbers by using the following format: (authors), J. Mater. Chem. A, (year), DOI: 10.1039/c6ta08233e.	
2	Please carefully check the spelling of all author names. This is important for the correct indexing and future citation of your article. No late corrections can be made.	
3	Please check that the Graphical Abstract text fits within the allocated space indicated on the front page of the proof. If the entry does not fit between the two horizontal lines, then please trim the text and/or the title.	

Journal of Materials Chemistry A

PAPER

A high-performance flexible and weavable asymmetric fiber-shaped solid-state supercapacitor enhanced by surface modifications of carbon fibers with carbon nanotubes†

Cite this: DOI: 10.1039/c6ta08233e

Xiaoyu Lu,[ab] Yang Bai,[a] Ranran Wang[a] and Jing Sun*[a]

Received 22nd September 2016
Accepted 25th October 2016

DOI: 10.1039/c6ta08233e

www.rsc.org/MaterialsA

To meet the demands of high energy storage and low productive cost as well as the ability to be incorporated into wearable electronics, we developed a flexible and weavable asymmetric fiber-shaped solid-state supercapacitor (a-FSSC) based on carbon fiber bundle@CNT–$NiCo(OH)_x$ (CF@CNC) and carbon fiber bundle@activated carbon (CF@AC) electrodes with increased operating voltage (1.4–1.6 V) and capacitance. For the positive electrode of CF@CNC, great electrochemical performance enhancement brought about by surface modifications with air plasma and carbon nanotube (CNT) coating is demonstrated. For the negative electrode of CF@AC, a facile and effective way of incorporating activated carbon into carbon fiber bundles is developed. The resultant assembled a-FSSC showed an areal energy and power density of 33.0 μW h cm^{-2} and 0.75 mW cm^{-2} at 1.6 V, which are better than those of most of the present fiber-shaped supercapacitors. The volumetric energy and power density of 0.84 mW h cm^{-3} and 19.1 mW cm^{-3} are also comparable to the reported results. Its long cycle life (100% capacitance retention after 8000 charge–discharge cycles) reveals its high electrochemical stability. High capacitance retention in the repeated bending (20% decay after 1000 bending times) and torsion (107% retention after 1000 twisting times) tests demonstrated the great flexibility, structural stability and potential utilization of the a-FSSC in wearable electronics. As a demonstration, a woolen fabric woven with three a-FSSCs connected in series can light a blue LED and be worn on the arm.

1. Introduction

A rapid development of flexible, wearable and stretchable electronic devices such as flexible sensors, artificial skin and portable devices has motivated the exploration for appropriate flexible energy supply.[1–3] Compared with traditional bulky and rigid energy storage devices, fiber-shaped solid state supercapacitors (FSSCs) have shown promising prospects in such personalized electronics thanks to their lightweight, flexibility, high power/energy densities, and long cycle life as well as ease of integration.[4,5] As for practical application, FSSCs can be readily woven into textiles to exhibit unique functions and even endowed with stretchability by incorporating a coiled structure.[6–8] The core challenge now is to increase the energy storage and power delivery of FSSCs and to maintain high flexibility when applied to various wearable devices.[1]

Usually, a FSSC is made of two fibrous electrodes with active materials on the surface assembled with a solid-state electrolyte. Since the fiber substrate plays a dominant role as both the current collector and support, many attempts have been made to develop carbonaceous fibers such as reduced graphene oxide (rGO) and carbon nanotube (CNT) fibers by wet-spinning, dry-spinning and other methods.[9–21] Along with directly used carbon fibers (CFs), they provide high electrical conductivity and endow the FSSC with intensity, flexibility and weavability.[22] To realize streamlining and standardization to meet the demands of mass production, Peng and his co-workers[23] proposed a continuous process by integrating the main four steps of FSSC fabrication: fiber substrate preparation, active material introduction, electrolyte infiltration and the assembly of the FSSC device. But concerning their cost, even with excellent electrical and capacitive properties, CNT and rGO fibers are currently too expensive as electrode substrates. Direct utilization of commercially available carbon fibers and metal wires (Ni,[24] Ti[25] *etc.*) seems to solve the problem by removing the first step of fiber substrate preparation. Metal wires with better

[a]*The State Key Lab of High Performance Ceramics and Superfine Microstructure, Shanghai Institute of Ceramics, Chinese Academy of Sciences, 1295 Ding Xi Road, Shanghai 200050, China. E-mail: jingsun@mail.sic.ac.cn; Fax: +86 21 52413122; Tel: +86 21 52414301*

[b]*University of Chinese Academy of Sciences, 19 Yuquan Road, Beijing 100049, PR China*

† Electronic supplementary information (ESI) available. See DOI: 10.1039/c6ta08233e

electrical conductivity than carbonaceous materials serve well as the current collector, but their low surface area limits the deposition amount of active materials. Besides, the FSSC built on metal wires can hardly meet the demands of repeated bending and lightweight for wearable electronics due to its inborn rigidity and relatively heavy weight.[26] Wang and his co-workers prepared a polyester yarn coated with Ni to obtain the flexibility of yarn as well as high electrical conductivity of Ni. But the preparation of hybrid fiber substrates is still quite complex.[27] As for these concerns, carbon fibers (CFs) are more promising in the near future because of their balanced properties of fine conductivity, great mechanical properties and low costs.

According to the equations for energy (E) and power (P) densities of an FSSC: $E = CV^2/2$, $P = E/t$, the performances of an FSSC can be improved through improving the capacitance (C) and extending the voltage window (V). One common approach is to coat the original fiber substrate with pseudocapacitive materials such as rGO,[27] polyaniline (PANI),[12] polypyrrole (PPy)[15,28] and transition metal oxides/hydroxides including manganese dioxide (MnO_2),[29,30] cobalt oxide (Co_3O_4),[20] $NiCo_2O_4$ (ref. 31) and so on. The introduction of pseudocapacitance has resulted in the poor capacitance of traditional electrical double layer capacitors. However, the relatively poor electrical conductivity and low specific surface area as well as the hydrophobic surface of CFs make them unfavorable for the deposition of active materials and effective ion/electron exchange,[24] resulting in poor electrochemical reactivity and structural instability such as cracking and exfoliation of the introduced active material.[32] As another approach, enlarging the operating voltage of FSSCs is effective in promoting their energy storage and output. For example, compared with symmetric supercapacitors, asymmetric ones can expand the operation voltage range from 0–0.6 V to 0–1.5 V with an energy density enhancement of 1860%.[24] Choosing suitable and efficient counter fiber electrodes for the positive electrode in FSSCs opens up a new research topic but has not yet been intensively investigated. Since the negative electrode in an asymmetric SC system usually requires a carbonaceous material with a high surface area, strategies such as electrochemical activation[33] and a modified Hummers' method[34] have been applied to endow pristine smooth CFs with partially exfoliated thin carbon sheets that are attached to the inner core. Nonetheless, these methods often include complex and time-consuming oxidation–reduction procedures. Considering these disadvantages, it is still a challenge to achieve well-designed CF-based electrodes for asymmetric FSSCs with high energy storage, lightweight and flexibility for applications in flexible and wearable electronics.

In order to combine these two approaches to gain high energy storage, we propose the fabrication of an asymmetric fiber-shaped solid-state supercapacitor (a-FSSC) made of CNT modified CF bundles electrodeposited with $NiCo(OH)_x$ (CF@CNC) as the positive electrode and activated carbon (AC) coated CFs (CF@AC) as the negative electrode. To overcome the intrinsic drawbacks of CFs such as hydrophobicity, relatively poor electrical conductivity and low surface area, air plasma treatment and CNT modification on the CF surface were applied during the fabrication of CF@CNC. The two strategies synergistically helped in establishing intimate interaction between the CF and the electrodeposited porous $NiCo(OH)_x$, not only improving the ion/electron transport on the interface but also preventing the deposited $NiCo(OH)_x$ from falling off during reactions. The negative electrode was prepared by readily incorporating carbon fiber bundles with activated carbon, revealing excellent capacitance and cyclic stability. Benefitting from its unique hierarchical porous structure and improved potential window (1.6 V), the CF-based a-FSSC exhibited areal and volumetric energy densities of 33.0 μW h cm^{-2} and 0.84 mW h cm^{-3}, respectively, which are superior to those of most of the reported FSSCs. Typically, an 8.5 cm long, 2.4 mm thick FSSC exhibited a capacitance of 400 mF at a high current density of 5 mA. The excellent flexibility and stability were further demonstrated with repeated bending and torsion tests. As the power supply for wearable electronics, a piece of cotton fabric woven with a-FSSCs can be worn on the arm while lighting up commercial light-emitting diodes (LEDs). Moreover, due to the facile fabrication of CF bundles, the a-FSSC can be readily tuned in thickness and length to meet various requirements for serving well as an ideal energy storage device for flexible and wearable electronics.

2. Experimental and calculation sections

2.1 Preparation of CF@CNC, CF@NC and CF@PNC

The CFs were drawn out from a commercial CF fabric and washed with deionized water and ethanol. A bundle of CFs with adjustable length and thickness was assembled using silver paste and copper tape to gain a CF electrode substrate. The pristine CF bundle was firstly treated with an air plasma system (manufactured by the Institute of Plasma Physics, Chinese Academy of Sciences) under a condition of 60 mW for 4 min in order to obtain a hydrophilic surface. The pretreated CF bundle was then dip-coated in a SWCNT aqueous solution (0.25 mg mL^{-1}, NanoIntegris) and dried in an electrical oven at 60 °C. This process was repeated once again for sufficient coating of CNTs. In an aqueous solution that contained $Ni(NO_3)_2$ (0.0075 M), $Co(NO_3)_2$ (0.0075 M) and urea (0.15 M), electrodeposition was conducted with a CF bundle as the working electrode, a platinum wire as the counter electrode and an SCE as the reference electrode. The CF working electrode was conducted at a constant potential of −0.9 V. The as-prepared CF@CNC was dried at room temperature. In the text, the average diameter of CF@CNC and CF@AC bundles is 0.92 mm (Fig. S1†) and the electrodeposition time is 25 min if not specially declared.

For comparison, the CF bundle without any special treatment before direct electrodeposition under the same conditions as the CF@CNC was denoted as CF@NC. The CF bundle treated with air plasma before the electrodeposition was denoted as CF@PNC.

2.2 Preparation of CF@AC

Activated carbon was mixed with acetylene black and polyvinylidene fluoride in ethanol in a weight ratio of 80 : 10 : 10 to

form a uniform slurry. A pristine CF bundle was dip-coated with the mixture slurry and dried at room temperature. The CF@AC was obtained after repeating the above process several times.

2.3 Fabrication of the a-FSSC

An a-FSSC was assembled with a CF@CNC (or contrast samples) and a CF@AC using PVA–KOH as the gel electrolyte. The PVA–KOH gel was prepared by dissolving 4 g PVA in 40 mL 2 M KOH solution and then heating at 90 °C for 1 h. Both the positive and negative electrodes were immersed in the electrolyte for 30 min at first, and then dried in air for 10 min. Subsequently, the two electrodes were twisted together to make an a-FSSC. After drying at room temperature, the device was subjected to various tests for the evaluation of its capacitance, flexibility and other performances.

2.4 Material characterization

The microstructure and morphology of the samples were characterized with a field emission scanning microscope (Hitachi UHR FE-SEM SU 8220) and a transmission electron microscope (JEM-2100F at 200 kV). Raman spectra were recorded on a DXR Raman Microscope, Thermal Scientific Corporation, USA, with a 532 nm excitation length. The resistances of CF and CF@C bundles were measured using a four-probe method at room temperature, which can eliminate the contact resistance between the CF bundle and probe. The contact angle was tested with an operation manual for an automatic contact angle meter (Kono, SL200B). In the repeated bending and torsion tests, a universal testing machine (CMT6103, MTS Systems (China) Co., Ltd.) was used to bend the a-FSSC to specific positions. And a 30° twisting angle was applied with a high-precision motorized rotation stage.

2.5 Electrical measurements of the single electrode and fiber supercapacitor

Electrochemical tests (linear sweep voltammetry, cyclic voltammetry, galvanostatic charge–discharge and Nyquist plots) were conducted with an electrochemical workstation CHI 660D. A three-electrode cell consisting of an SCE electrode as the reference electrode, a platinum wire as the counter electrode, and CF-based electrodes as the working electrode in a 2 M aqueous KOH electrolyte was used to evaluate the electrochemical performances. The individual fiber electrodes were about 920 μm in diameter and 8.5 cm in length if not specially declared. The CF-based electrode as a whole is considered as a cylinder to calculate its surface area (A_{fiber}) and volume (V_{fiber}). Specific areal capacitance (C_{sp}) measured in the three-electrode system was calculated by

$$C_{\text{sp}} = C_{\text{electrode}}/A_{\text{fiber}} \quad (1)$$

where $C_{\text{electrode}}$ is the measured capacitance of the fiber electrode calculated from CV curves according to the following formula:

$$C_{\text{electrode}} = \frac{Q}{2V} = \frac{1}{2V\nu}\int i(V)\mathrm{d}V \quad (2)$$

in which Q represents the total voltammetric charge of a CV curve, V is the operating potential window, ν is the scan rate and $i(V)$ is the current density.

The performances of the assembled a-FSSC were evaluated in a two-electrode configuration. Nyquist plots were obtained under open circuit voltage at frequencies from 100 000 to 1 Hz, with a potential perturbation of 5 mV.

The capacitance of a-FSSCs (C_{cell}) was calculated from galvanostatic charge–discharge curves according to the formula:

$$C_{\text{cell}} = \frac{it}{V - V_{\text{IR}}} \quad (3)$$

in which i represents the discharging current, t is the discharging time, V is the operating voltage and V_{IR} is the IR drop. The capacitance calculated from CV curves was based on the formula:

$$C_{\text{cell}} = \frac{1}{2V\nu}\int i(V)\mathrm{d}V \quad (4)$$

where V represents the operating voltage, ν is the scan rate and $i(V)$ is the current density.

The specific areal capacitance of the a-FSSC was calculated by dividing capacitance by the total surface area of the two electrodes in the device:

$$C_{\text{A}} = C_{\text{cell}}/A_{\text{cell}} \quad (5)$$

The capacitances normalized to length (C_{cell}, L) and volume (C_{cell}, V) could be obtained in the same way. The device volume refers to the sum of two cylindrical fiber electrodes coated with the gel electrolyte. The diameter of the CF-based electrode increased to about 1200 μm after electrolyte coating.

The areal/volumetric energy density of the a-FSSC was calculated from galvanostatic charge–discharge curves by the formula:

$$E_{\text{A/V}} = \frac{1}{2}C_{\text{A/V}}(V - V_{\text{IR}})^2 \quad (6)$$

where $V - V_{\text{IR}}$ is the actual operating voltage window.

The areal/volumetric power density of the a-FSSCs was calculated by the formula:

$$P_{\text{A/V}} = E_{\text{A/V}}/t \quad (7)$$

in which t refers to the discharging time.

3. Results and discussion

3.1 Preparation and characterization of the positive electrode CF@CNC

The preparation route of the CF@CNC and the fabrication of the a-FSSC are illustrated in Scheme 1. A CF bundle is composed of numerous CFs (~7.0 μm in diameter) with a smooth surface (Fig. 1a). Due to the hydrophobic surface of CFs, the aqueous solution containing the CNT and electrodeposition solution can hardly be soaked into the CF bundle. Fig. 1b shows the

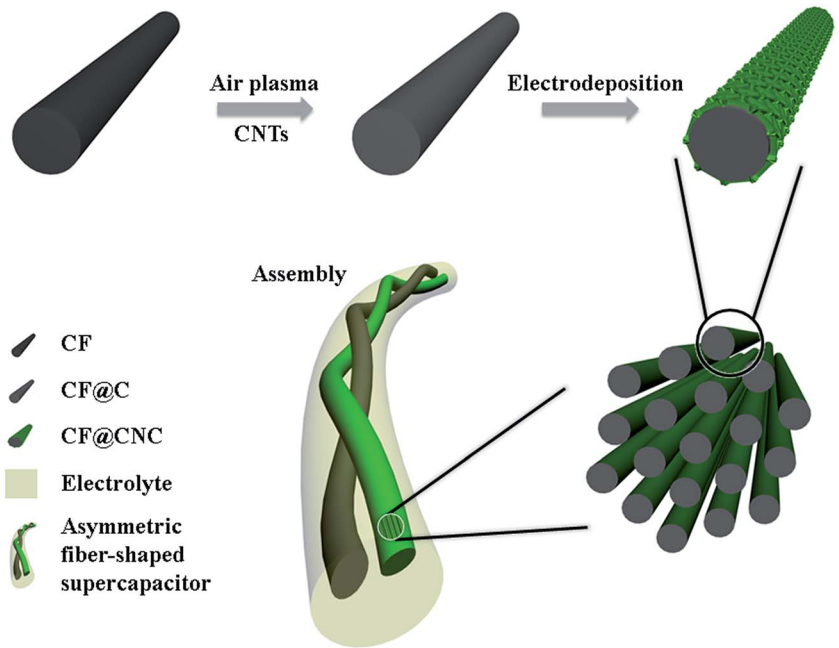

Scheme 1 Schematic illustration of the synthesis procedure for the CF@CNC and fabrication of the asymmetric fiber-shaped solid-state supercapacitor.

morphology of the CF@NC sample. Because of bad wetting, the deposited $NiCo(OH)_x$ is uneven. Some area is more deposited and turn into a densely packed structure, while the rest of the area is less deposited. After air plasma treatment, the contact angle of the CF bundle decreased from 135° to 0° (Fig. S2†), implying that the CF surface is effectively decorated with hydrophilic groups. Compared with other chemical pretreatments, air plasma has advantages such as time-saving and good repeatability. Moreover, air plasma treatment can 'clean' the CF surface thoroughly, which is commonly used in industrial production. As a result, the surface of CF@PNC (Fig. 1c) shows an even honeycomb morphology constructed with vertically aligned $NiCo(OH)_x$ nanosheets, with pore size ranging from 50 to 200 nm (Fig. 1d). Since the electrochemical reactions in a supercapacitor essentially rely on the active sites,[35] the deposited porous $NiCo(OH)_x$ with a large surface area would improve the capacitive performances.

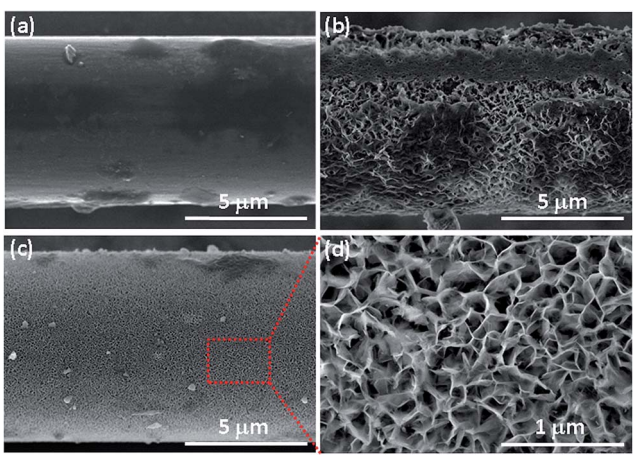

Fig. 1 (a–c) SEM images of a CF, CF@NC and CF@PNC, respectively; (d) high-resolution SEM image of CF@PNC. CF@NC and CF@PNC are electrodeposited for 25 min.

To further improve the CF properties by surface modification, we coated CFs with a thin layer of CNTs after air plasma treatment (denoted as CF@C). As shown in Fig. 2a, the CF@C is similar to the original CF in a low resolution. In a high resolution (Fig. 2b), CNTs with random orientations are observed on the CF surface. The first advantage of CNT modification is the improved electrical conductivity. The linear resistance of a typical bundle was reduced from 4.4 Ω cm^{-1} to 2.4 Ω cm^{-1} after CNT decoration. The second advantage of CNT modification is the enhanced ion diffusion ability. Although the amount of CNTs can hardly be measured by using a precision balance, they have an obvious impact on the electrodeposited $NiCo(OH)_x$. Under the same electrodeposition conditions and with a similar amount of active material with CF@PNC, the $NiCo(OH)_x$ nanosheets in the CF@CNC exhibit a different morphology (Fig. 2c). On one hand, CNTs on the smooth CF surface create more active sites for electrodeposition.[36] On the other hand, the CF surface is divided by CNTs into small regions. Within these confined regions, the deposited $NiCo(OH)_x$ nanosheets become smaller. They tend to pile up and finally grow obliquely instead of vertically, forming a different honeycomb structure with shrunken pores (40–80 nm) (Fig. 2d). As a result, the deposited layer of $NiCo(OH)_x$ on CF@CNC (~0.06 μm) is much thinner than that on CF@PNC (~0.38 μm) according to the measured diameters of a single CF-based fiber in different samples (Table S1†). In the electrochemical reaction, the reduced thickness of the $NiCo(OH)_x$ layer

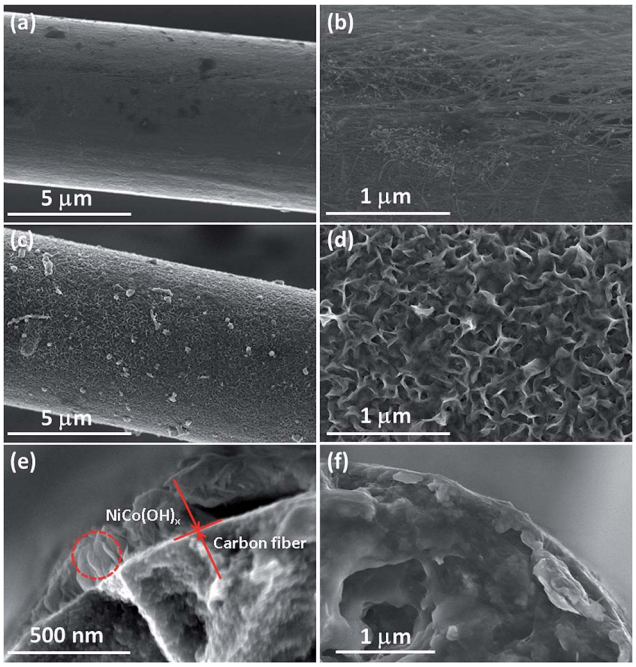

Fig. 2 (a) SEM image of the CF@C; (b) high-resolution SEM image of the surface of CF@C; (c) SEM image of the CF@CNC electrodeposited for 25 min; (d) high-resolution SEM image of the surface of CF@CNC; (e and f) cross-sectional views of CF@PNC and CF@CNC, respectively.

would greatly improve the capacitance of CF@CNC by shortening the ion diffusion length. Furthermore, as revealed in the cross-sectional views (Fig. 2e and f), a distinct boundary between the CF and electrodeposited $NiCo(OH)_x$ is observed in CF@PNC, showing that the porous $NiCo(OH)_x$ layer constructed by vertically aligned nanosheets is loosely anchored on the CF surface. In contrast, the inconspicuous interface of CF@CNC demonstrates the third advantage of CNT modification that induces tight interactions between the $NiCo(OH)_x$ and CF, not only improving the electron transport but also preventing the active material from falling off.

The compositions of the CF, CF@C, CF@PNC and CF@CNC electrodes were characterized with Raman spectroscopy and TEM and SEM observations. Exfoliated $NiCo(OH)_x$ nanosheets with some wrinkles are shown in Fig. 3a. The selected area electron diffraction (SAED) pattern reveals a diffraction ring corresponding to the (101) facet of $Co(OH)_2$ (JCPDS 45-0031) and $Ni(OH)_2$ (JCPDS 14-0117). The vague ring pattern implies the low crystallinity due to electrodeposition preparation. Raman spectra (Fig. 3b) of the CF and CF@PNC exhibit the existence of D bands (1360 cm^{-1}) and G bands (1590 cm^{-1}) that are attributed to the CF. The multiple peaks of CF@PNC at the low Raman shift reveal the A_{1g} vibration (around 460 cm^{-1}) and E_g vibration (around 550 cm^{-1}) modes of Ni–Co hydroxides.[37,38] As for the CF@C, the strong peaks at 175 cm^{-1}, 1597 cm^{-1} and 2680 cm^{-1} are typical peaks of CNTs, which are debilitated a little in the spectrum of CF@CNC due to the coverage of $NiCo(OH)_x$ electrodeposited on CF@C. The spectrum of CF@CNC indicates the coexistence of the CF, CNTs and $NiCo(OH)_x$. According to the EDS maps of CF@CNC (Fig. S3†), elements Ni and Co are evenly distributed on the surface, suggesting the simultaneous electrodeposition of Ni and Co hydroxides. Through the elemental analysis (Table S2†), the molar ratio of Ni/Co is measured to be 0.72 : 1, close to the ratio (1 : 1) in the electrodeposition electrolyte. The concentrations of $Ni(NO_3)_2$, $Co(NO_3)_2$ and urea that greatly influence the deposited material have been adjusted according to a study we have reported.[37] Ni–Co double hydroxides with an optimized Ni/Co ratio would exhibit much greater capacitive performance as well as cyclic stability.

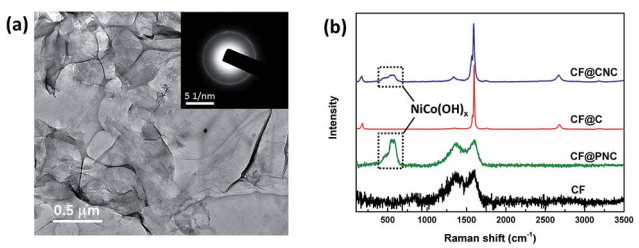

Fig. 3 (a) TEM image of the exfoliated $NiCo(OH)_x$ with the corresponding SAED pattern in the inset; (b) Raman spectra of the CF, CF@PNC, CF@C and CF@CNC.

3.2 Electrochemical performances of the CF@CNC

The as-prepared CF-based hybrid fibers were directly used as the working electrode in a three electrode system to evaluate their electrochemical performances. Cyclic voltammetry tests were conducted at a scan rate of 5 mV s^{-1} in a potential window of −0.4 V to 0.6 V. For comparison, all the electrode samples in this test were electrodeposited for 25 min and the measured masses of active materials were comparable. As shown in Fig. 4a, the CF and CNTs contributed little to the total capacitance. After being electrodeposited with $NiCo(OH)_x$, the CF@NC, CF@PNC and CF@CNC show typical pseudocapacitive behaviors with a pair of oxidation and reduction peaks. The CF@PNC showed a higher capacitance than CF@NC because the hydrophilic treatment induced uniformly electrodeposited $NiCo(OH)_x$ and better contact with the CF. It is noteworthy that the capacitance of CF@CNC nearly doubled that of CF@PNC with the incorporation of the CNT interface layer. The great enhancement is due to (i) the highly conductive network on the CF surface brought about by CNTs that accelerates electron transport, (ii) the relatively dense honeycomb structure of $NiCo(OH)_x$ with reduced thickness that shortens the ion diffusion length, and (iii) enhanced interaction between $NiCo(OH)_x$ and the CF.

As another important factor, the influence of electrodeposition time was also investigated. SEM images of CF@CNC electrodeposited with increasing time are shown in Fig. S4.† In the first 10 minutes of electrodeposition, numerous $NiCo(OH)_x$ whiskers lay flat on the CF surface, indicating an intimate interaction. Then a porous layer composed of small $NiCo(OH)_x$ flakes was grown on the dense layer. With prolonged time for more than 40 minutes, the flakes and pores became larger. These images imply a hierarchical structure of

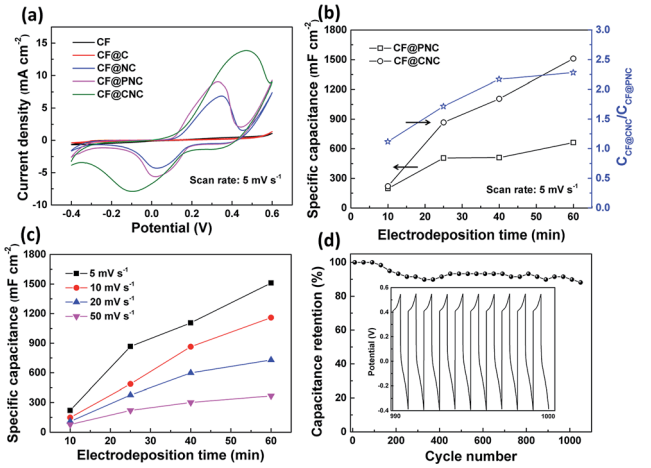

Fig. 4 Electrochemical performances of the positive electrode fibers tested in a three-electrode system. (a) CV curves of the CF, CF@C, CF@NC, CF@PNC and CF@CNC electrodeposited for 25 min at a scan rate of 5 mV s^{-1}; (b) capacitances calculated from CV curves of CF@PNC and CF@CNC with different electrodeposition times and capacitance ratios of CF@CNC to CF@PNC; (c) capacitances calculated from CV curves of CF@CNC at different scan rates; (d) cyclic galvanostatic charge–discharge stability of the CF@CNC at a current density of 16 mA cm^{-2}.

$NiCo(OH)_x$ in CF@CNC with a dense interior and porous exterior. The specific capacitances of CF@PNC and CF@CNC electrodes deposited for 10 to 60 minutes are compared in Fig. 4b. The two electrodes deposited for 10 min showed similar performances (145 mF cm^{-2} for CF@PNC (10 min) and 162 mF cm^{-2} for CF@CNC (10 min)). The capacitances of the CF@CNC electrodes increased almost linearly with respect to the deposition time from 10 to 60 min (1110 mF cm^{-2} for CF@CNC (60 min)). Supposing that the amount of active material is proportional to the electrodeposition time, the deposited $NiCo(OH)_x$ in CF@CNC had all taken part in the redox reactions. However, the capacitance of CF@PNC only increased to 2.3 fold when the deposition time was 6 times as long, with the $C_{CF@CNC}/C_{CF@PNC}$ value increasing monotonously from 1.1 to 2.3. At the start of electrodeposition (10 min), the deposited amount of $NiCo(OH)_x$ in both samples was small enough to fully react, leading to comparable capacitances. But the capacitance of CF@PNC has little increment when the deposition time exceeded 25 min. This is a common phenomenon of deficient reactivity of active materials caused by poor electron/ion transport and loose contact with the fiber substrate. Such weakness has been overcome by CNT modification. In addition, the CNT layer in CF@CNC works as a sort of 'adhesive' additive to prevent the $NiCo(OH)_x$ from falling off. As revealed in Fig. S5,† a part of deposited $NiCo(OH)_x$ in CF@PNC has exfoliated after 10 CV cycles, exposing the smooth CF surface, which is barely seen in the CF@CNC. After 1000 charge–discharge cycles (Fig. 4d) CF@CNC still showed 90% capacitance retention. As a result, the CF@CNC fiber bundle with high specific capacitance, good rate capability (Fig. 4c) and prolonged cycle life is a promising candidate as the positive electrode for FSSCs.

3.3 Preparation and electrochemical performances of the negative electrode CF@AC

In an asymmetric supercapacitor, the overpotential brought about by the negative electrode material, such as activated carbon (AC) and rGO, results from reversible hydrogen electrosorption in nanoporous carbon-based materials. Considering the complexity of preparing rGO[23,24] and the oxidation–reduction activation methods,[33,34] we proposed a facile way to prepare carbon fiber-based negative electrodes by simply coating carbon fiber bundles with AC-containing slurry. Considering the hydrophobic nature of AC, air plasma treatment was not applied for better adhesion of AC particles on the CF surface. SEM images at different magnifications of the as-prepared CF@AC are shown in Fig. 5. Numerous AC composite nanoparticles disperse well and anchor on the CF surface, with some relatively large aggregated particles lying in between the CFs. We performed electrochemical measurements in a three electrode system with CF@AC as the working electrode. A stable potential window was observed in the range from −1.0 V to 0 V for CF@AC, demonstrating that the a-FSSC can be operated up to 1.6 V (Fig. 6a–c). Moreover, the CF@AC electrode exhibits excellent rate capability (Fig. 6d and e) and cyclic stability (98% capacitance retention after 1000 cycles at 8 mA cm^{-2}, Fig. 6f) owing to the effective AC functionalization of CFs. Based on the specific capacitances and potential windows for both electrodes, the mass ratio of the positive and negative electrodes was fixed at around 1 : 16 (Fig. S6†).

3.4 Electrochemical performances of the a-FSSC

To make full use of the enhanced specific capacitance of CF@CNC and the expanded potential window of CF@AC, the a-FSSC was fabricated by combining the two fiber electrodes. The electrochemical performances of the a-FSSC were investigated in a two-electrode configuration. Fig. 7a shows the CV curves of the a-FSSC measured at different operation voltages from 1.4 V to 1.8 V. In all voltage ranges, the presence of redox peaks demonstrated the pseudocapacitive behavior of the capacitor that originated from the positive electrode (CF@CNC). When the operation potential was gradually extended to 1.8 V, larger peak currents were observed, indicating more faradic reactions owing to the negative electrode.[39] Besides, the charge–discharge curves of the a-FSSC at a current density of 2.0 mA cm^{-2} showed a typical *I*–*V* response with similar charging and discharging time (Fig. 7b). An extended voltage window from 1.4 V to 1.8 V meanwhile improved the specific capacitance (Fig. S7†), and

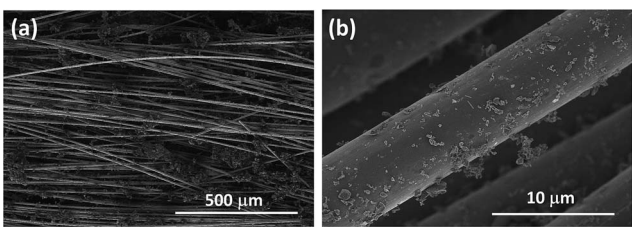

Fig. 5 (a and b) SEM images of the CF@AC at different magnifications.

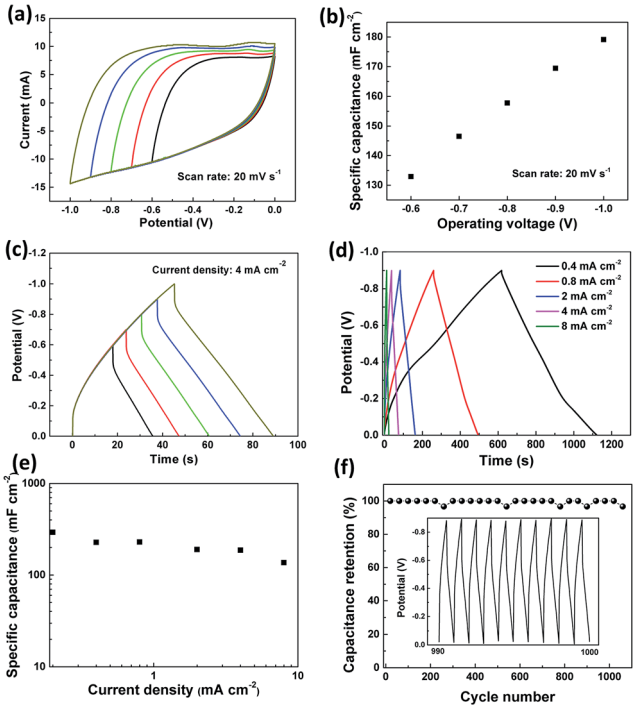

Fig. 6 Electrochemical performances of the CF@AC negative electrode fibers tested in a three-electrode system. (a) CV curves measured in a potential window ranging from −0.6 V to −1.0 V and (b) the corresponding capacitances calculated from the CV curves; (c) GCD curves of the CF@AC with different operating potential windows; (d) GCD curves at current densities ranging from 0.4 to 8.0 mA cm^{-2} of the CF@AC in the potential window of −0.9 to 0.0 V; (e) capacitances calculated from GCD curves as a function of the current density; (f) cyclic performance of the CF@AC at a current density of 8.0 mA cm^{-2}.

thus enhanced energy storage is obtained according to $E = CV^2/2$. The CV curves were measured with a scan rate from 5 mV s^{-1} to 100 mV s^{-1} (Fig. 7c). Galvanostatic charge–discharge (GVD) curves of the a-FSSC at current densities from 1.0 to 8.0 mA cm^{-2} are shown in Fig. 7d. The discharge plateaus in the curves indicate a pseudocapacitive feature of the a-FSSC. IR drops of the a-FSSC with respect to current densities fitted well in a linear function, showing a quiet low internal resistance of about 25 Ω (Fig. S8†). As shown in Fig. 7e, the specific areal (linear) capacitance of the a-FSSC operated at 1.4 V and 1.0 mA cm^{-2} was measured to be 111 mF cm^{-2} (64.0 mF cm^{-1}), which remains to be 31.9 mF cm^{-2} (18.4 mF cm^{-1}) when raising the current density up to 8.0 mA cm^{-2}. With great rate capability, a typical a-FSSC with a capacitance of 156 mF can be fully charged within 2 seconds. These capacitance values were better than those of many reported fiber-shaped supercapacitors, such as rGO–Ni-yarn SCs (49.4 mF cm^{-2} and 8.9 mF cm^{-1} at 1.0 mA cm^{-2})[27] and CNT@Co_3O_4 yarn-based SCs (52.6 mF cm^{-2} at 0.053 mA cm^{-2}).[20] The excellent rate capability and energy storage proves that the CNT layer and the deposited hierarchical $NiCo(OH)_x$ provide fast electron/ion transport and the large electrolyte/electrode interface for electrochemical reactions. Stable cyclic performance was achieved at 6 mA cm^{-2} with an operation voltage of 1.4 V. During the first 2000 cycles, the capacitance gradually increased probably due to the slow infiltration of the solid-state electrolyte and activation of the active material. After 8000 charge–discharge cycles, the a-FSSC retained as much as 103% of its initial capacitance (Fig. 7f). The coulombic efficiency defined as the discharging time over charging time ratio increased and remained at above 90% during the long-term cycles. In addition, with an operation voltage of 1.6 V, it also exhibited 110% retention of its original capacitance after 5000 cycles (Fig. S9†) with a similar increasing trend of the capacitance. However, when the voltage was extended to 1.8 V, the a-FSSC failed within hundreds of cycles. Irreversible reactions of the electrodes and deterioration of the gel electrolyte are possible reasons for the failure. As a result, the a-FSSC has a stable performance below 1.6 V. In a durability test, the a-FSSC was wrapped with a plastic film and kept at room temperature and moisture before the GCD test. It turns out that the capacitance showed a steady increment along with time for similar reasons mentioned above. After more than 15 days, the a-FSSC retains 130% of its initial capacitance (Fig. 7g). The excellent performance retention demonstrates its highly reversible reactions and unique stable structures of the CF@CNC and CF@AC. EIS measurements were performed to evaluate the internal resistances of the a-FSSC (Fig. 7h). After 3000 GCD cycles, the equivalent series resistance (ESR) of the device increased a little from 5.8 Ω to 6.4 Ω, while the charge transfer resistance dropped obviously, which revealed enhanced contact between the electrolyte and fiber electrodes during the cycles. The Ragone plot shown in Fig. 7i compares the areal performance of the a-FSSC with that of other reported FSSCs. At 1.4 V, the a-FSSC exhibited a maximum energy density of 25.1 μW h cm^{-2} with the power density of 0.48 mW cm^{-2}. At 1.6 V, the energy density further increased to 33.0 μW h cm^{-2} with the power density of 0.75 mW cm^{-2}. These values of the a-FSSCs are superior to those of most of the reported fiber-shaped SCs, such as ones made from CNT/rGO composite fibers (3.8 μW h cm^{-2}),[23] activated CF tows (3 μW h cm^{-2}),[34] MnO_2/CNT/nylon fibers (2.6 μW h cm^{-2}),[7] PPy@MnO_2@rGO conductive yarns (9.2 μW h cm^{-2}),[6] Ni–rGO yarns (1.6 μW h cm^{-2}),[27] wet-spinning rGO/CNT fibers (3.84 μW h cm^{-2}),[40] confined hydrothermal rGO fibers (0.17 μW h cm^{-2})[9] and wet-spinning PANI/CNT fibers (0.56 μW h cm^{-2}),[41] but lower than the SC made of CNT–PPy–HQ fibers (98 μW h cm^{-2}).[15] Moreover, the results normalized to the total volume of the a-FSSC (0.84 mW h cm^{-3} and 19.1 mW cm^{-3}) are also comparable to those of the reported supercapacitors (Fig. S10†). Therefore, the a-FSSC is a promising fiber-shaped supercapacitor with high energy storage and cyclic performance.

3.5 Mechanical properties and practical use of the a-FSSC

To demonstrate the flexibility and mechanical stability of the a-FSSC that are of great importance to wearable electronics applications, the capacitances derived from the GCD and CV curves were recorded under different deformations. The original CF bundle exhibited a measured tensile strength of up to 233 MPa (Fig. S11†). Such great mechanical strength was supposed to be inherited from the carbon fiber-based

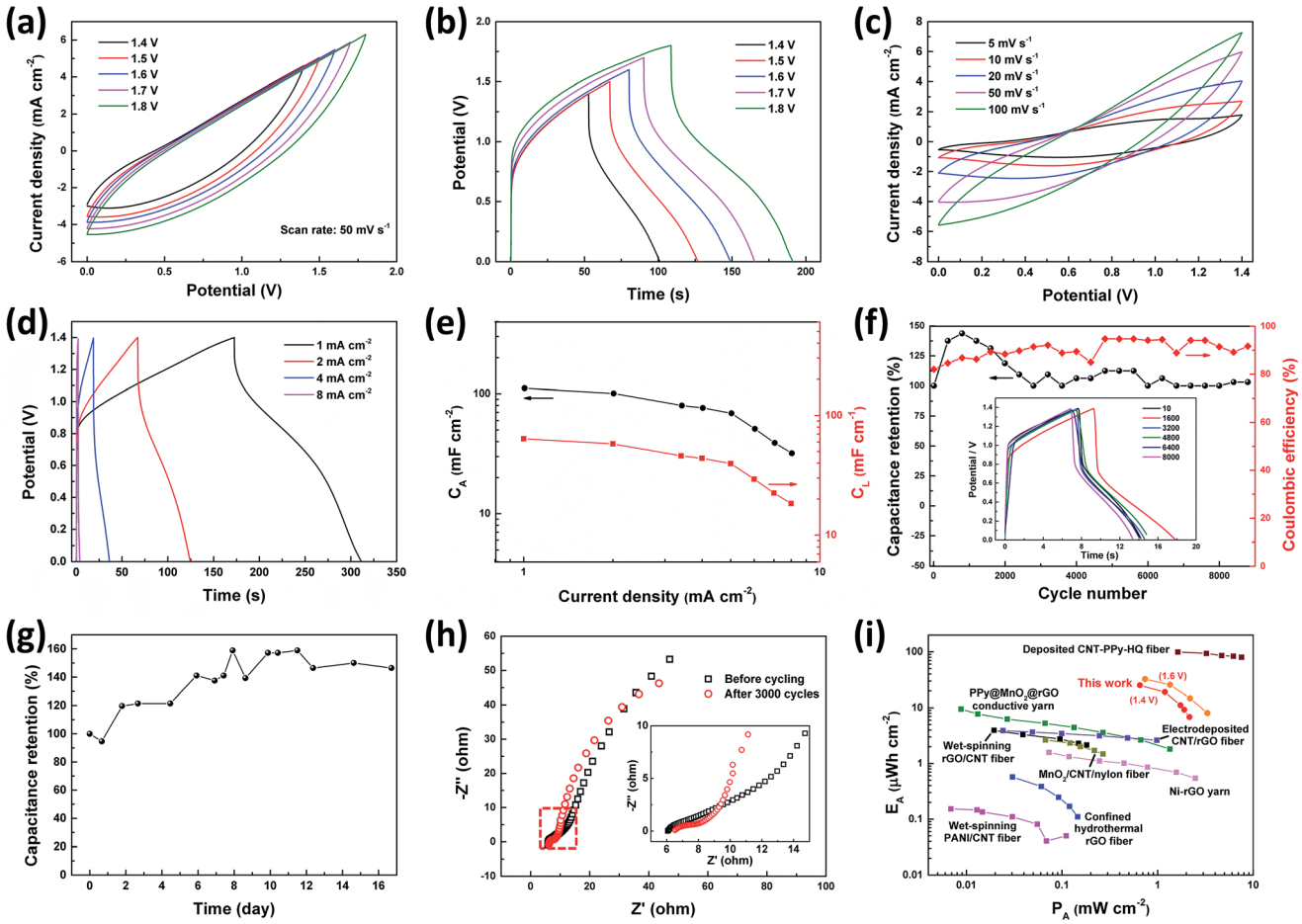

Fig. 7 Electrochemical performances of the a-FSSC tested in a two-electrode system. (a) CV curves and (b) GCD curves of the a-FSSC with different operating potential windows; (c) CV curves with scan rates between 5 and 100 mV s^{-1} and (d) GCD curves at current densities ranging from 1.0 to 8.0 mA cm^{-2} of the a-FSSC in the potential window of 0.0–1.4 V; (e) areal and linear capacitances calculated from GCD curves as a function of the current density; (f) cyclic GCD test of the a-FSSC at a current density of 4.0 mA cm^{-2} with calculated capacitance and coulombic efficiency values during the cycles; (g) capacitance retention of the a-FSSC with respect to preserving time; (h) Nyquist plots with a frequency range from 100 kHz to 1 Hz for the a-FSSC before and after 3000 charge–discharge cycles; (i) Ragone plot comparing the areal energy density and power density with previously reported studies.

electrodes. As shown in Fig. 8b, under a bending angle below 90°, the capacitance slightly increased to 104% possibly because of the improved contact between the fiber electrode and gel electrolyte.[27] When bent to 180°, the a-FSSC still retains 95% of its initial capacitance. Since the CF bundle is composed of numerous CFs with different lengths, some CFs shorter than the whole device (~8.5 cm) may partly disconnect from the other CFs in the bundle. Furthermore, a repeated bending test was performed for the a-FSSC. 80% capacitance retention was observed after bending (Fig. 8c) 1000 times with the coulombic efficiency remaining at above 90% during the cycles. Considering the relatively large size of the fibrous electrode in diameter (1.2 mm compared with tens to hundreds of millimeters in the most reported cases), the large inner stress in the bending state may cause detachment between the electrode and electrolyte, resulting in the capacitance loss. The a-FSSC was further twisted for 30° 1000 times with one end fixed and the other end attached to a rotation motor. The inset of Fig. 8d shows that the CV curve of the a-FSSC has little changes after repeated torsion. The high capacitance retention (107%) is attributed to the entangled pattern of the two-fiber electrode that sustains torsion stress. The CNT layer in the positive electrode also helps to retain the capacitance during the deformations by making active materials adhere to carbon fibers.

Practical use has various requirements for high voltage or high capacitance. The a-FSSCs can be connected in series or parallel to enlarge the output voltage or operating current, respectively. Five supercapacitors connected in series showed a charging/discharging window of 7.0 V with similar charging and discharging time (Fig. 9a). The measured capacitances of the series-connected a-FSSCs dropped linearly with the reciprocal of the number of capacitors (Fig. 9b). As for parallel connection, with an enhancement of scanning current, the capacitances calculated from CV curves increased linearly with the number of capacitors (Fig. 9c and d).

Considering the weavability of the a-FSSC, three of them were connected in series and integrated into a piece of fabric knitted with common cotton yarns, as shown in Fig. 9e. After

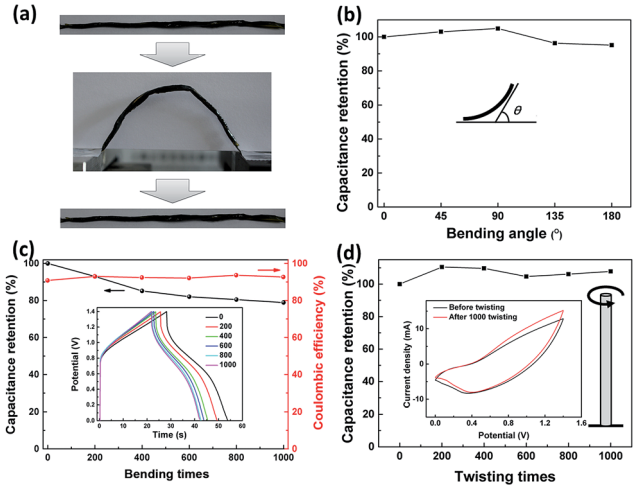

Fig. 8 (a) Digital images of the a-FSSC at bending and releasing states during the repeated bending test; (b) capacitance retention of the a-FSSC under different bending angles; (c) capacitance retention and coulombic efficiency changes of the a-FSSC during repeated bending–releasing cycles at a current density of 2 mA cm^{-2}. The inset shows the charge–discharge curves during the reciprocating moves; (d) capacitance retention of the a-FSSC during repeated twisting–releasing cycles (torsion angle 30°) at a scan rate of 20 mV s^{-1}. The inset shows the CV curves before and after 1000 twisting times.

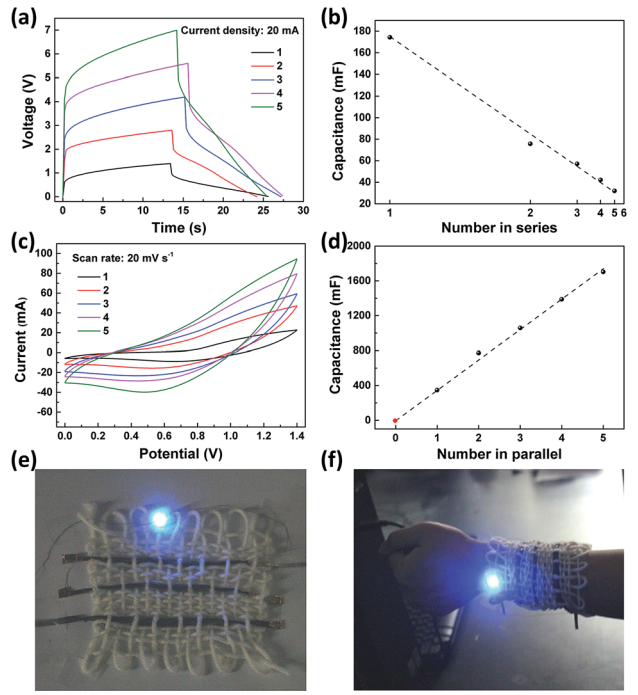

Fig. 9 (a) Charge–discharge curves at a current density of 4 mA cm^{-2} of one to five a-FSSCs connected in series and (b) the corresponding capacitance with respect to the number of supercapacitors. (c) CV curves with a scan rate of 20 mV s^{-1} of one to five a-FSSCs connected in parallel and (d) the corresponding capacitance with respect to the number of supercapacitors. (e) Digital image of a blue LED lit by three a-FSSCs connected in series woven into a woolen fabric and (f) a demonstration of the fabric wore on an arm.

being fully charged, this energy-storing fabric can light a blue light-emitting diode (LED) with a working voltage above 2.5 V (Fig. S12 and Movie S1†). Owing to the demonstrated flexibility and weavability of the a-FSSC, this fabric can be freely bent and worn on the arm meanwhile lighting the blue LED (Fig. 9f). Furthermore, the a-FSSC can be tuned in length and thickness for various requirements (Fig. S13†), which is realized by twining different amounts of carbon fibers into a bundle. Therefore, the a-FSSC would meet the need for high energy and power densities and weavability of flexible electronics in the future.

4. Conclusions

In summary, we have fabricated a flexible and weavable asymmetric fiber-shaped solid-state supercapacitor based on carbon fibers. In the positive electrode of CF@CNC, plasma treatment and introduction of a CNT interlayer have induced faster electron transport, shortened ion diffusion length and intimate contact between CFs and the electrodeposited $NiCo(OH)_x$, leading to improved capacitance and structural stability. By facilely incorporating hydrophobic CFs with activated carbon composite slurry, the negative electrode of CF@AC also exhibits great electrochemical performance. The assembled a-FSSC displays high areal and volumetric energy/power density and excellent long-term cyclic stability, which can be attributed to the good electrochemical reactivity and structural stability of both electrodes. Owing to the great mechanical properties of the CF, the a-FSSC shows great flexibility and capacitance retention during 1000 times of different deformations. By virtue of its high energy/power density, superior flexibility, ease of scalable production and tunable size, the a-FSSC would have wide applications in portable devices, smart electronics, implantable medical devices and so on. This work specially demonstrates the importance of interfacial modification between the fiber current collector and active material, which is applicable to most of the fiber-shaped solid-state supercapacitors.

Acknowledgements

This work is financially supported by the National Natural Science Foundation of China (Grant No. 61301036, 51402340) and Youth Innovation Promotion Association CAS (2014226).

References

1 S. Pan, J. Ren, X. Fang and H. Peng, *Adv. Energy Mater.*, 2016, **6**, 1501867.
2 W. Zeng, L. Shu, Q. Li, S. Chen, F. Wang and X. M. Tao, *Adv. Mater.*, 2014, **26**, 5310–5336.
3 X. Lu, M. Yu, G. Wang, T. Zhai, S. Xie, Y. Ling, Y. Tong and Y. Li, *Adv. Mater.*, 2013, **25**, 267–272.
4 P. Yang and W. Mai, *Nano Energy*, 2014, **8**, 274–290.
5 D. Yu, Q. Qian, L. Wei, W. Jiang, K. Goh, J. Wei, J. Zhang and Y. Chen, *Chem. Soc. Rev.*, 2015, **44**, 647–662.
6 Y. Huang, H. Hu, Y. Huang, M. Zhu, W. Meng, C. Liu, Z. Pei, C. Hao, Z. Wang and C. Zhi, *ACS Nano*, 2015, **9**, 4766–4775.

7 C. Choi, S. H. Kim, H. J. Sim, J. A. Lee, A. Y. Choi, Y. T. Kim, X. Lepro, G. M. Spinks, R. H. Baughman and S. J. Kim, *Sci. Rep.*, 2015, **5**, 9387.

8 Y. Shang, C. Wang, X. He, J. Li, Q. Peng, E. Shi, R. Wang, S. Du, A. Cao and Y. Li, *Nano Energy*, 2015, **12**, 401–409.

9 Y. Meng, Y. Zhao, C. Hu, H. Cheng, Y. Hu, Z. Zhang, G. Shi and L. Qu, *Adv. Mater.*, 2013, **25**, 2326–2331.

10 J. Ren, W. Bai, G. Guan, Y. Zhang and H. Peng, *Adv. Mater.*, 2013, **25**, 5965–5970.

11 J. Ren, L. Li, C. Chen, X. Chen, Z. Cai, L. Qiu, Y. Wang, X. Zhu and H. Peng, *Adv. Mater.*, 2013, **25**, 1155–1159.

12 K. Wang, Q. Meng, Y. Zhang, Z. Wei and M. Miao, *Adv. Mater.*, 2013, **25**, 1494–1498.

13 L. Wen, F. Li and H. M. Cheng, *Adv. Mater.*, 2016, **28**, 4306–4337.

14 S. Pan, J. Deng, G. Guan, Y. Zhang, P. Chen, J. Ren and H. Peng, *J. Mater. Chem. A*, 2015, **3**, 6286–6290.

15 R. Xu, F. Guo, X. Cui, L. Zhang, K. Wang and J. Wei, *J. Mater. Chem. A*, 2015, **3**, 22353–22360.

16 S. Chen, W. Ma, Y. Cheng, Z. Weng, B. Sun, L. Wang, W. Chen, F. Li, M. Zhu and H.-M. Cheng, *Nano Energy*, 2015, **15**, 642–653.

17 G. Huang, C. Hou, Y. Shao, B. Zhu, B. Jia, H. Wang, Q. Zhang and Y. Li, *Nano Energy*, 2015, **12**, 26–32.

18 F. Su and M. Miao, *Nanotechnology*, 2014, **25**, 135401.

19 D. Yu, K. Goh, H. Wang, L. Wei, W. Jiang, Q. Zhang, L. Dai and Y. Chen, *Nat. Nanotechnol.*, 2014, **9**, 555–562.

20 F. Su, X. Lv and M. Miao, *Small*, 2015, **11**, 854–861.

21 D. Zhang, M. Miao, H. Niu and Z. Wei, *ACS Nano*, 2014, **8**, 4571–4579.

22 C.-F. Sun, H. Zhu, E. B. Baker III, M. Okada, J. Wan, A. Ghemes, Y. Inoue, L. Hu and Y. Wang, *Nano Energy*, 2013, **2**, 987–994.

23 B. Wang, X. Fang, H. Sun, S. He, J. Ren, Y. Zhang and H. Peng, *Adv. Mater.*, 2015, **27**, 7854–7860.

24 X. Wang, B. Liu, R. Liu, Q. Wang, X. Hou, D. Chen, R. Wang and G. Shen, *Angew. Chem.*, 2014, **53**, 1849–1853.

25 X. Li, X. Li, J. Cheng, D. Yuan, W. Ni, Q. Guan, L. Gao and B. Wang, *Nano Energy*, 2016, **21**, 228–237.

26 Y. Huang, Y. Huang, M. Zhu, W. Meng, Z. Pei, C. Liu, H. Hu and C. Zhi, *ACS Nano*, 2015, **9**, 6242–6251.

27 X. Pu, L. Li, M. Liu, C. Jiang, C. Du, Z. Zhao, W. Hu and Z. L. Wang, *Adv. Mater.*, 2016, **28**, 98–105.

28 W. Liu, N. Liu, Y. Shi, Y. Chen, C. Yang, J. Tao, S. Wang, Y. Wang, J. Su, L. Li and Y. Gao, *J. Mater. Chem. A*, 2015, **3**, 13461–13467.

29 X. Xiao, T. Li, P. Yang, Y. Gao, H. Jin, W. Ni, W. Zhan, X. Zhang, Y. Cao, J. Zhong, L. Gong, W. C. Yen, W. Mai, J. Chen, K. Huo, Y. L. Chueh, Z. L. Wang and J. Zhou, *ACS Nano*, 2012, **6**, 9200–9206.

30 L. Dong, C. Xu, Y. Li, C. Wu, B. Jiang, Q. Yang, E. Zhou, F. Kang and Q. H. Yang, *Adv. Mater.*, 2016, **28**, 1675–1681.

31 W. Xiong, X. Hu, X. Wu, Y. Zeng, B. Wang, G. He and Z. Zhu, *J. Mater. Chem. A*, 2015, **3**, 17209–17216.

32 J. Wang, X. Li, Y. Zi, S. Wang, Z. Li, L. Zheng, F. Yi, S. Li and Z. L. Wang, *Adv. Mater.*, 2015, **27**, 4830–4836.

33 H. Jin, L. Zhou, C. L. Mak, H. Huang, W. M. Tang and H. L. W. Chan, *Nano Energy*, 2015, **11**, 662–670.

34 D. Yu, S. Zhai, W. Jiang, K. Goh, L. Wei, X. Chen, R. Jiang and Y. Chen, *Adv. Mater.*, 2015, **27**, 4895–4901.

35 C. Zhu, P. Yang, D. Chao, X. Wang, X. Zhang, S. Chen, B. K. Tay, H. Huang, H. Zhang, W. Mai and H. J. Fan, *Adv. Mater.*, 2015, **27**, 4566–4571.

36 H. Kuan-Xin, W. Quan-Fu, Z. Xiao-gang and W. Xin-Lei, *J. Electrochem. Soc.*, 2006, **153**, A1568.

37 Y. Bai, W. Wang, R. Wang, J. Sun and L. Gao, *J. Mater. Chem. A*, 2015, **3**, 12530–12538.

38 S. R. Shieh and T. S. Duffy, *Phys. Rev. B: Condens. Matter Mater. Phys.*, 2002, **66**, 134301.

39 P. Sun, Z. Deng, P. Yang, X. Yu, Y. Chen, Z. Liang, H. Meng, W. Xie, S. Tan and W. Mai, *J. Mater. Chem. A*, 2015, **3**, 12076–12080.

40 L. Kou, T. Huang, B. Zheng, Y. Han, X. Zhao, K. Gopalsamy, H. Sun and C. Gao, *Nat. Commun.*, 2014, **5**, 3754.

41 Q. Meng, K. Wang, W. Guo, J. Fang, Z. Wei and X. She, *Small*, 2014, **10**, 3187–3193.